

Supplementary Information

In-situ Grown, Self-Supported Iron-Cobalt-Nickel Alloy Amorphous Oxide Nanosheets with Low Overpotential toward Water Oxidation

Jiaqi Fan, Zuofeng Chen, Huijie Shi, Guohua Zhao*

Department of Chemistry, Shanghai Key Lab of Chemical Assessment and Sustainability,

Tongji University, 200092 Shanghai, China

*To whom correspondence should be addressed. E-mail address: g.zhao@tongji.edu.cn

Contents

A. Experimental Section

B. Supplementary Results

C. Supplementary References

A. Experimental Section

The ternary and binary alloy oxides were prepared by one-step anodization at of FeCoNi alloys (Scheme 1) at a cell voltage of 50 V in a mixed solution of 1:1 (v/v) ethylene glycol (EG) and glycerol (GLY) with 3 M H₂O and 0.54 M NH₄F at 5°C or room-temperature (RT) for 8 h with stirring. The sizes of all ternary and binary alloy plate were 3 cm × 1 cm, and the anodization area was remain to 1 cm × 1 cm. Before annealing, the anodized alloy plate was rinsed with deionized water, and dried in the N₂ stream. And then, the plate was immersed into the deionized water for 2 h, and dried in the N₂. Finally, repeat the rinsing and drying process once more.

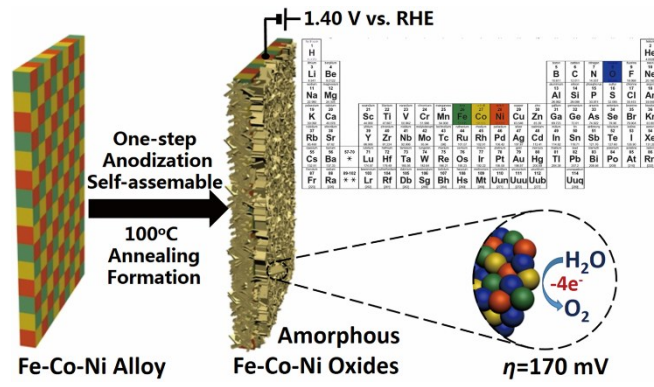
The FeCoNi alloys were purchase from Institute of metal research, Chinese academy of sciences. The ternary alloy was product by smelting process with 1: 1: 1 (mol / mol) Fe (Purity, ≥ 99.9%): Co (Purity, ≥99.8%): Ni (Purity, ≥99.9%) and no other additive. Ethylene glycol, glycerol, NH₄F and all the other chemicals and organic solvents used were analytical grade (Sigma-Aldrich Co., Ltd.). All aqueous solutions were prepared with deionized water.

For the synthesis of electrodes, Pt plate was used as a cathode. The as-prepared electrodes were annealed in air for one hour at different temperatures (100°C, 300°C, and 500°C) using a furnace. The FTO/FeCoNiO_x were prepared by photochemical metal-organic deposition (PMOD) according to the literature.¹

The polarization measurements were carried out by a computer controlled electrochemical system (CHI 660) in a three-electrode compartment electrochemical cell at (298±1) K with a sweep rate of 10 mV s⁻¹ in 0.1 M KOH at room temperature with LSV and CV curves. Electrochemical impedance spectroscopy (EIS) was used to determine the conductivity of electrode with the

frequency range from 1×10^5 to 1×10^{-3} Hz and amplitude 5 mV at the open-circuit potential, and the electrolyte was 0.1 M KOH solution. The pH value of the electrolyte solution was measured to be 12.6. All potentials reported were iR-compensated. The counter electrode compartment, containing a platinum electrode and an Ag/AgCl (sat. KCl) reference electrode was placed in the third compartment, attached to the working electrode compartment with a Luggin capillary.

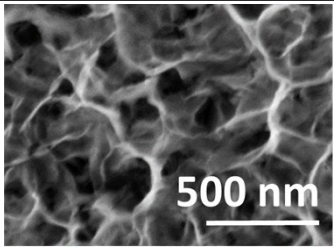
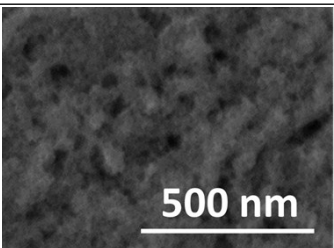
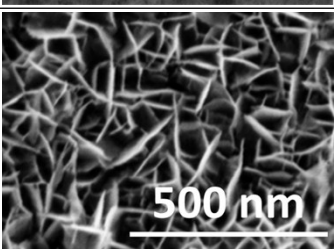
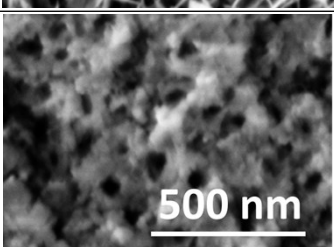
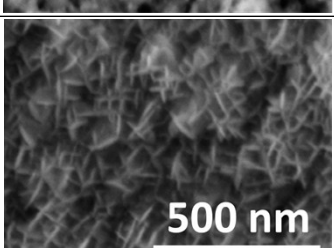
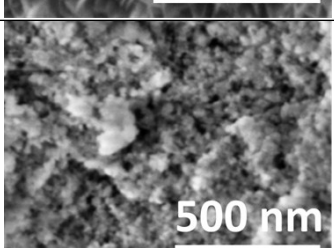
The morphology was analyzed with a scanning electron microscope (SEM) and Energy dispersive spectroscopy (EDS) equipped with FE-SEM, Hitachi S-4800, Japan. Raman spectra were recorded on a Rainshaw inVia reflex Raman spectrometer using an infrared excitation laser source at the wavelength of 785 nm. The profile and roughness measurements were carried out from stereoscopic images using MeX software (Alicona). The samples were characterized by powder X-ray diffraction (XRD, Bruker D8 Advance diffractometer, Germany) with Cu K α 1 radiation ($\lambda = 1.5406 \text{ \AA}$, 40 kV, 100 mA) at a scanning speed of 3° min^{-1} over a 2θ range of $30\text{-}80^\circ$. The UV-vis diffuse reflectance absorption spectra (UV-vis DRS) were recorded by Avaspec-DRS UV-Vis absorbance spectrometer (Avantes, Netherlands). The X-ray photoelectron spectroscopy (XPS) measurements were performed on an AXIS Ultra HSA (Kratos Analytical Ltd, UK) X-ray photoelectron spectrometer with an Mg K α source. The contact angle of water on the electrode surface was examined by a contact angle meter (KRÜSS, Germany).



Scheme S1. Illustration of the fabrication of iron-cobalt-nickel oxide for water oxidation.

B. Supplementary Results

Table S1 Overview of parameters screening: A summary of the electrolyte compositions, anodization conditions and the resulting morphology of the obtained iron-cobalt-nickel alloy oxides. (EG: ethylene glycol; GLY: glycerol; EG/GLY: ethylene glycol 50% (v/v) and glycerol 50% (v/v); RT: room temperature).

Samples	Solvent	Electrolyte		Voltage (V)	T (°C)	SEM image
		NH4F (M)	H2O (M)			
A	EG	0.54	3	50	5	
B	EG	0.54	3	50	RT	
C	EG/GLY	0.54	3	50	5	
D	EG/GLY	0.54	3	50	RT	
E	GLY	0.54	3	50	5	
F	GLY	0.54	3	50	RT	

As shown by the SEM image of Sample C in Table S1, at 5°C when the precursor solution was composed of EG/GLY 1/1 (v/v), the prepared FeCoNiO_x showed a porous structure. The wall of pore, as nanosheet-like, could be formed uniformly with a length of approximately 100 nm and a width of 8-10 nm. The porous sample prepared in EG precursor solution at 5°C had more wider pore wall, about 80-120 nm. When the anodization precursor solvent was changed to GLY, the length of pore wall decreased to 60-70 nm, and the width also was thinner to 3-5 nm. The nanostructure of FeCoNiO_x nanosheets would greatly increase the electrode/electrolyte contact area, thus enhancing the electrochemical performance. However, by simply changing the temperature of anodization while keeping other conditions constant, the morphology of FeCoNiO_x changed from nanosheets-like to irregular structure, due to fierce water oxidation under room temperature (RT). We speculate that the solvents, EG and GLY, may play an important role as structure-directing-like agents in reforming the morphology during the anodization process. It is thought the reasons of nanostructure formed may be explained as the following: firstly, the proportion of metal components could influence the morphology of amorphous material surface. In reported, the different ratio of Fe/Ni would cause distinct microstructure of amorphous FeNi oxides, such as flower-like or sphere². On the other hand, the F element in anodization solution played an important role as corrosion and punching agent during the anodization process, and the nanosheets were walls of pores and holes after punching affection at original mother plate itself, not crystallinely deposited in the alloy substrate³. Our preparation method is “top to down”, and the metal element originates from mother alloy, different from “bottom to up” methods, with no need to introduce external metal element. It could avoid metal oxides crystalline growth caused by external metal element deposited on the substrate. In addition, the morphology of the electrode surface is also dependent on the operation temperature. When the operation temperature was set to RT and left uncontrolled, the electrode surface was rough without any characteristic nanostructures due to fierce water oxidation.

As shown by the UV-vis diffuse reflectance spectra in Fig. S1, the alloy oxide electrode treated in solvent of 100% EG can absorb visible light with the optical profile close to that of hematite (α - Fe_2O_3).⁴ Among these spectra, the alloy anodized in the solvent of EG/GLY 1:1 at 5°C exhibits a lowest visible light absorption. Fig. S1 shows that the alloy oxide formed at RT exhibits absorption in a wider wavelength range in comparison to that at 5 °C. As known, the amorphous catalyst was proved to be superior in OER performance than their crystalline form. Some metal oxides which have ability of visible light absorption, like Fe_2O_3 , Co_3O_4 , would lose the OER ability completely when they were fabricated as amorphous materials.^{1,5} For comparing the electrodes anodization in different anodization solutions, the electrochemical characterization of the samples anodized in EG, GLY, and EG/GLY at 5°C and annealed at 100°C were tested. It can be seen in Fig. S1b, the electrochemical performances of the NiCoFe ternary oxide prepared in EG/GLY was compared to that of the alloy metal oxides in EG and GLY (Fig. S2b). As can be seen, the catalytic onset appears at 1.44 V versus RHE for the sample prepared in GLY, which is 40 mV more positive than that of FeCoNiO_x prepared in EG/GLY. The catalytic activity of both the electrodes anodized in GLY and EG were sluggish than that of the electrode prepared in EG/GLY. The Tafel slopes for the materials fabricated in GLY and EG are in the range from 58 to 82 mV dec^{-1} and a current density of 5 mA cm^{-2} requires overpotentials from 210 mV to 270 mV, both larger than that of the electrode prepared in EG/GLY. We hope to get optimum conditions to prepare the materials with best electrochemical ability. The following studies on electrocatalysis are based on electrodes obtained under these conditions to ensure that the catalytic activity originates exclusively from amorphous oxides. And the electrode anodized in EG+GLY at 5°C with lowest visible light absorption and highest electrochemical ability was chosen to employ as our OER catalyst.

Figure S1

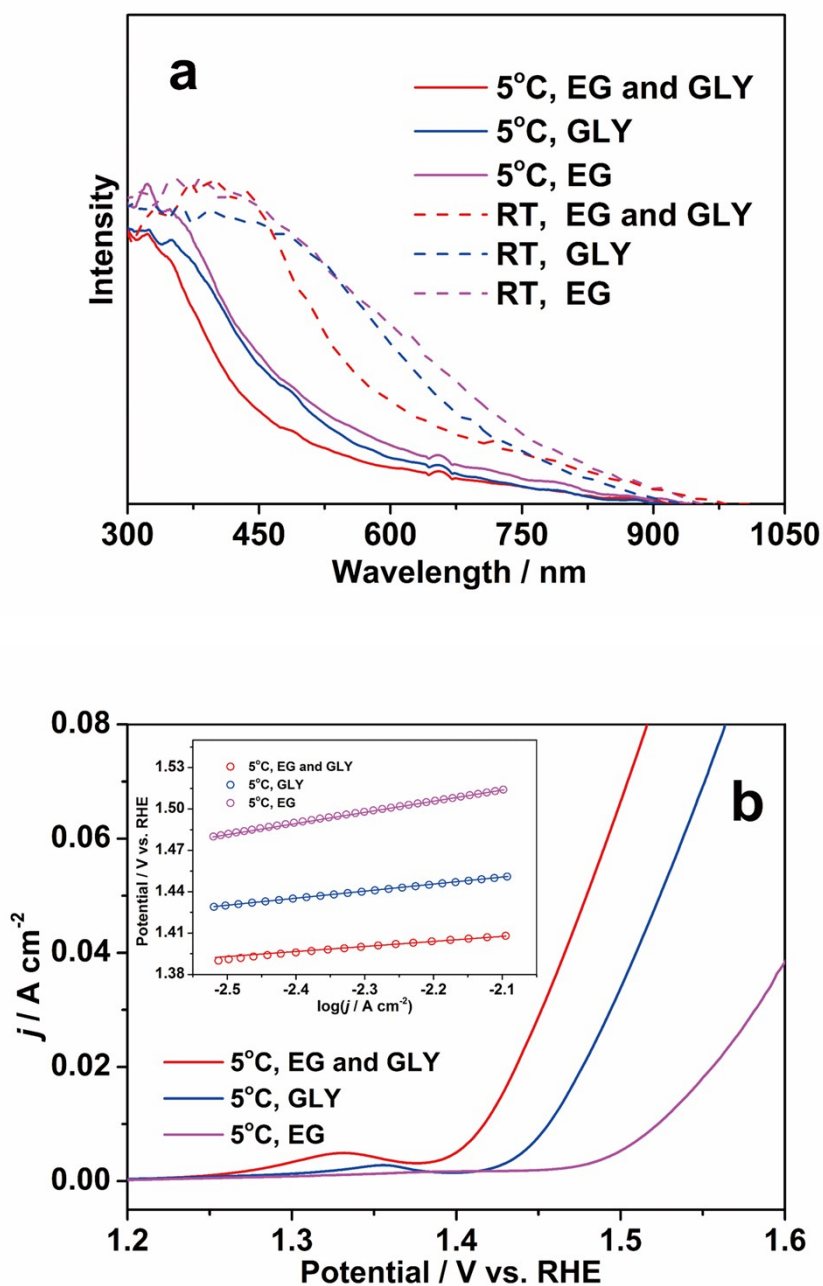


Figure S1 (a) Ultraviolet-visible (UV-vis) diffuse reflectance spectra for FeCoNiO_x electrodes by different anodization condition: variation of solvent compounds (v/v) (EG: ethylene glycol; GLY: glycerol) and at changing of operation temperature cell voltage of 50 V for 8 h. (b) Polarization (LSV) curves and Tafel plots (inset) of FeCoNiO_x electrodes in different anodization solutions (the anodization conditions are all set at a cell voltage of 50 V for 8 h by as solvent at 5°C and annealed at 100°C).

Figure S2

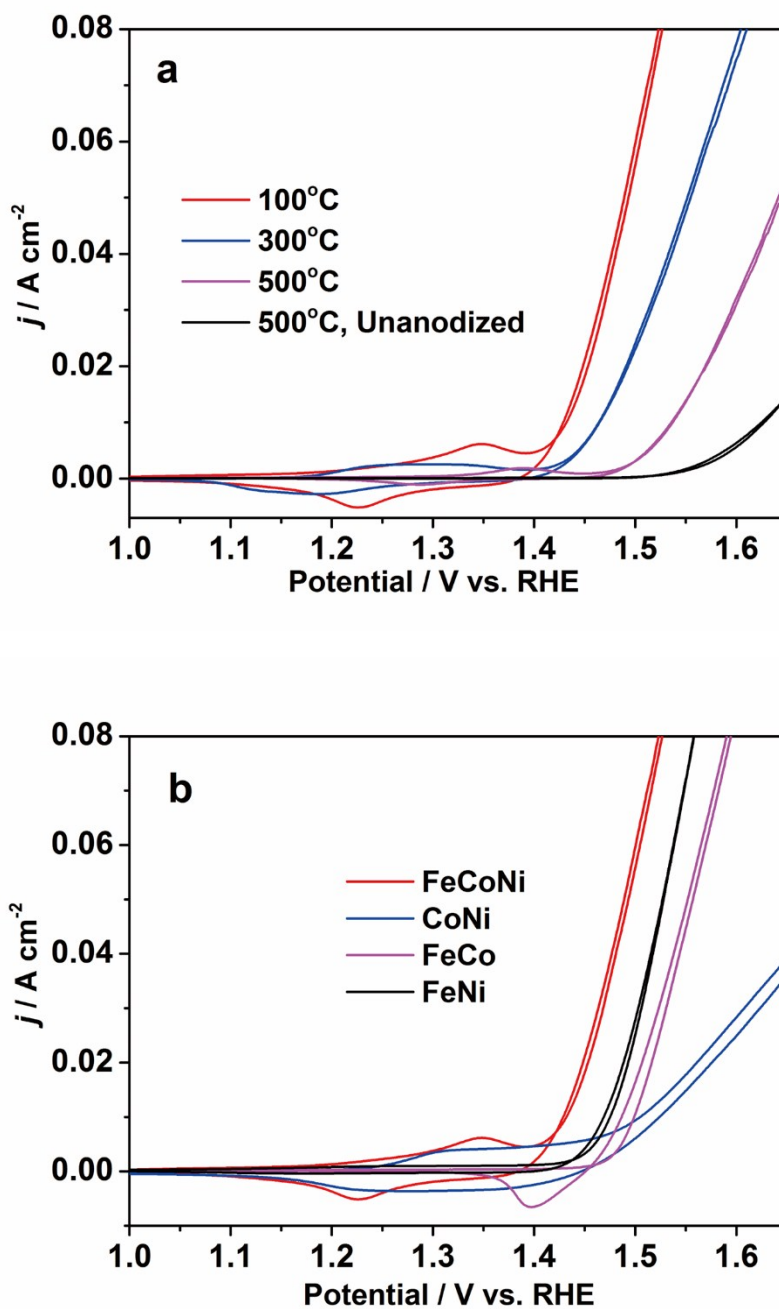


Figure S2 The cyclic voltammogram of (a) FeCoNiO_x electrodes under different fabrication condition (the anodization conditions are all set at a cell voltage of 50 V for 8 h by using EG/GLY (1:1, v:v) as solvent at 5°C) and (b) electrodes of different compounds (the anodization conditions are all set at a cell voltage of 50 V for 8 h by using EG/GLY (1:1, v:v) as solvent at of 5°C and annealeds at 100°C).

Figure S3

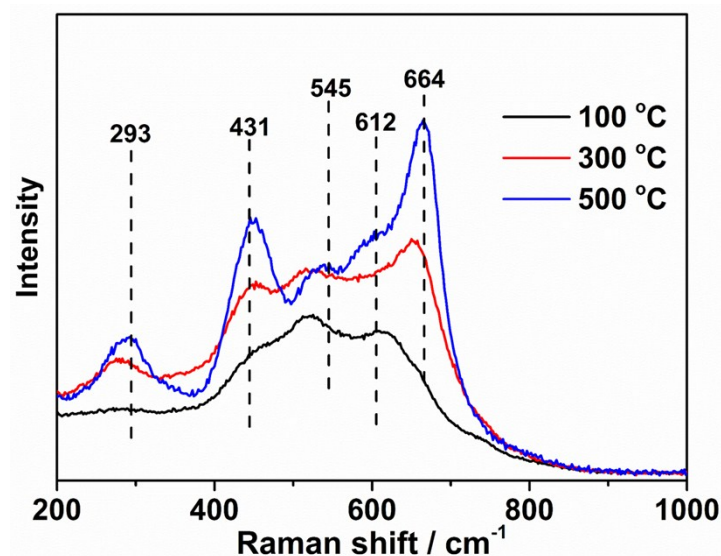
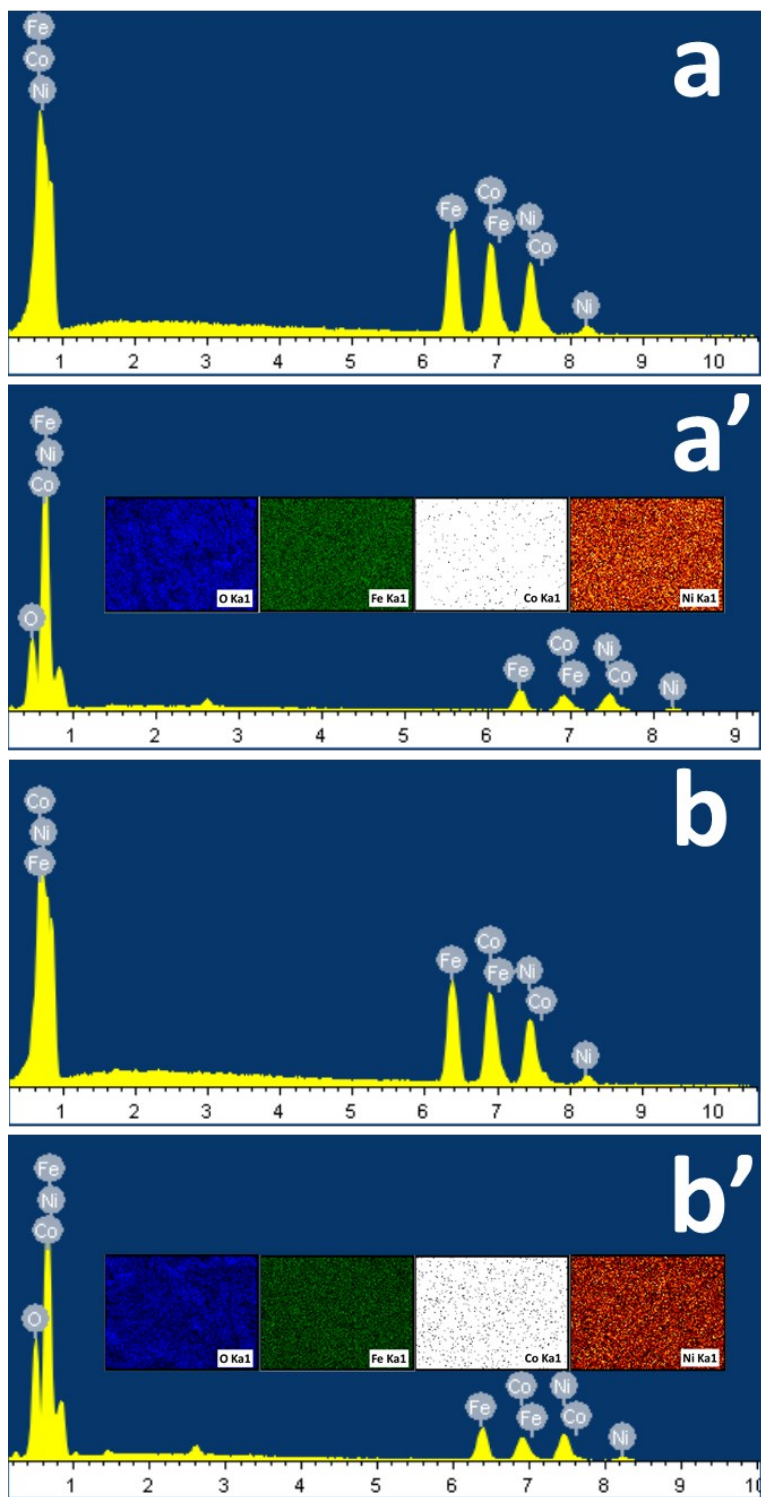


Figure S3 Raman spectra for FeCoNiO_x electrodes by different anneal temperature at 50 V cell voltage for 8 h by using EG/GLY (1:1, v/v) as solvent at 5°C.

The degree of crystallization was certainly different as indicated from the Raman spectra (Fig S3). Raman spectrum peaks of the positions at 293 cm⁻¹, 431 cm⁻¹, 612cm⁻¹ and 664cm⁻¹ are the characteristic Raman peaks of α -Fe₂O₃.⁶ The peaks observed at 545 cm⁻¹ is the characteristic peaks of Co₃O₄.⁷

Energy dispersive spectroscopy (EDS, Fig S4) analysis was performed to evaluate the relative content of different elements. At $T_{\text{anneal}} < 500$ °C, the elemental distributions for all FeCoNiO_x samples are close to their original ratios prior to annealing with only slight increase in Ni content (Tables S2 and S3). However, the percentage of iron dramatically rose after 500 °C annealing which is at the cost of the nickel content. This observation is arising from the difference in surface energy among these metals which leads to the enrichment of certain metals on the surface and others in the interior. The thermodynamic steady state of the particle surface is known to be dependent on the external conditions, such as temperature, that offer a chance to vary the surface composition.⁸

Figure S4



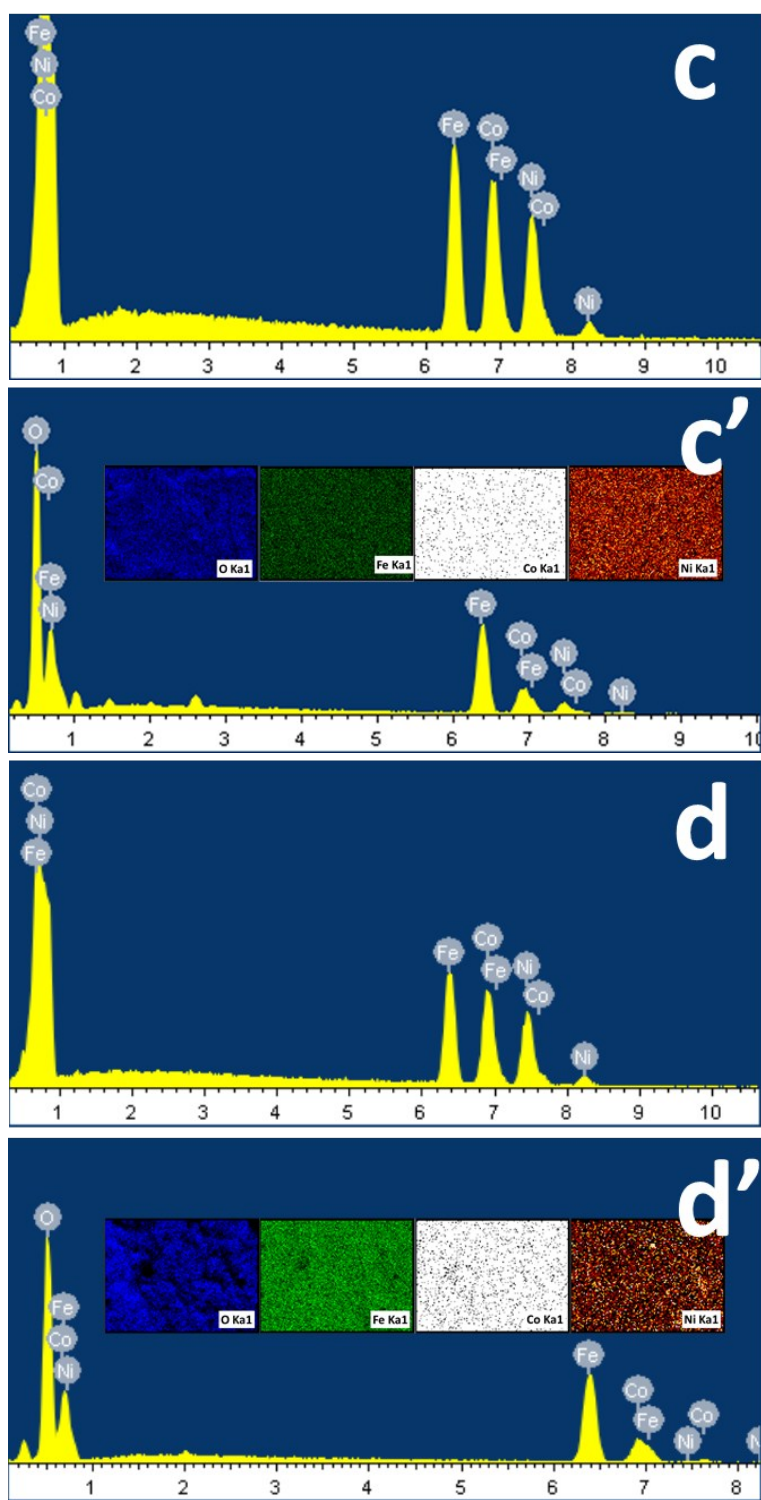


Figure S4 EDS for unprepared FeCoNi alloy (a, b, c, d) and prepared FeCoNiO_x electrodes by different condition (a', anodized, annealed 100°C; b', anodized, annealed 300°C; c', anodized, annealed 500°C; d', unanodized, annealed 500°C); EDS element mapping for prepared FeCoNiO_x electrodes by different condition (a' inset, anodized, annealed 100°C; b' inset, anodized, annealed 300°C; c' inset, anodized, annealed 500°C; d' inset, unanodized, annealed 500°C).

Figure S5

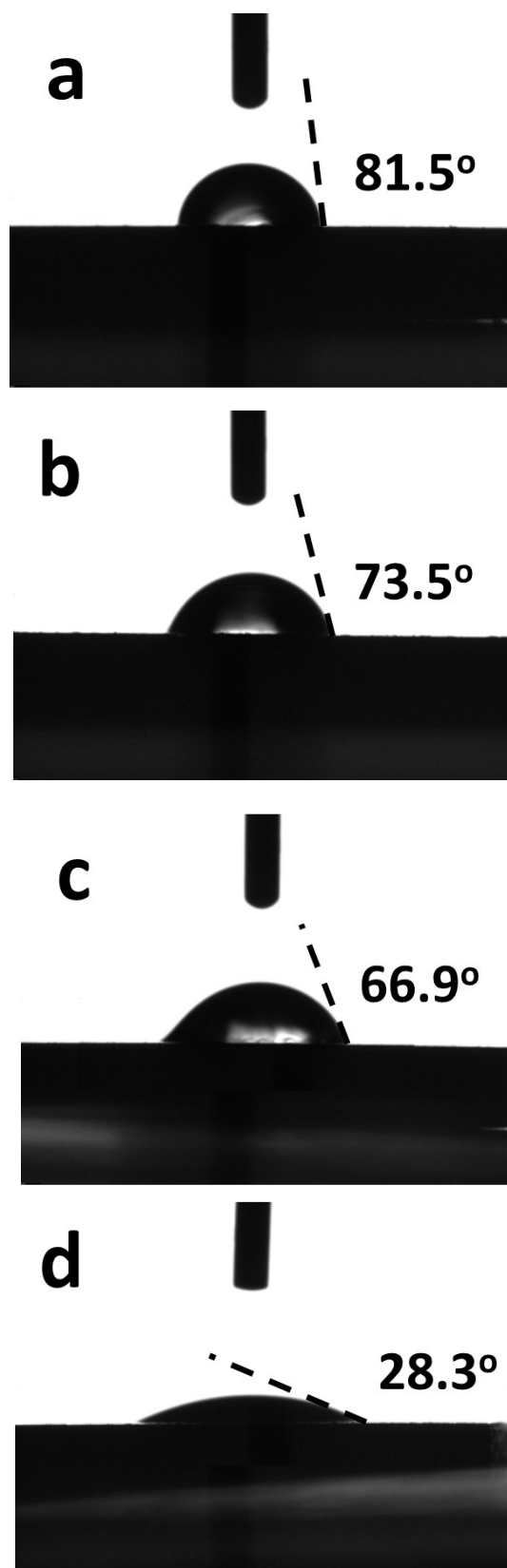


Figure S5 Contract angle (CA) for unprepared FeCoNi alloy (a) and prepared FeCoNiO_x electrodes by different condition (b, anodized, annealed 100°C; c, anodized, annealed 300°C; d, anodized, annealed 500°C).

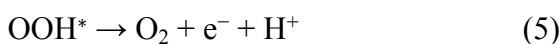
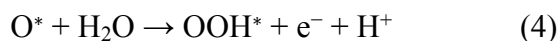
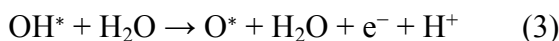
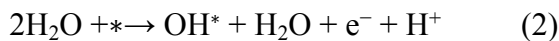
As known, the key of heterogeneous catalysis is that the catalyst must have strong capability of reactant adsorption to maintain rapid reaction rate. So the OER electrodes also need high absorption to water. The contact angles (θ_Y) test was performed to investigate the water adsorption capability of the materials. From Fig. S5, it can be seen that the contact angles of unprepared mother alloy plate was 81.5°. After anodized and annealed, the contact angles of the three electrodes were 73.5° (anodized, annealed 100°C), 66.9° (anodized, annealed 300°C), and 28.3° (anodized, annealed 500°C), all smaller than 90°.

The water either spreads or forms discrete droplets, when a small amount of water resides on the solid surface. This behavior is governed by the water surface energy γ , the surrounding gas and the solid, as a force balance between the solid-gas (γ_{sg}), solid-liquid (γ_{sl}) and liquid-gas (γ_{lg}) surface energy⁹:

$$\cos(\theta_Y) = (\gamma_{sg} - \gamma_{sl}) / \gamma_{lg} \quad (1)$$

Surfaces with $\theta_Y < 90^\circ$ are commonly called hydrophilic for water.¹⁰ It implies that all the anodized alloy electrodes presented hydrophilicity, in favor of water adsorption. And the adsorption of H₂O molecules onto the active sites was very crucial to improve the water oxidation ability.

At the same times, the water oxidation proceeded according to the following mechanism¹¹:



However, the reaction (2) and (3) means the catalysts must have some certain capability of water desorption, when they were hydrophilic. High water-solid surface energy enhanced water desorption. It required relatively higher liquid-solid surface energy between hydrophilic electrode and water. According to equation (1), the water-solid surface energy of the catalyst annealed at 100°C was greater than the two other anodized electrodes. So the catalyst annealed at 100°C had the biggest contact angle, but OER capability was remarkable. It was consistent with the literature¹² that the optimal catalyst bound neither too strong nor too weak with the reactant (H₂O), which was typically referred to as the Sabatier Principle.

Table S2 Elements composition of the untreated FeCoNi alloys (a, b, c, and d are all untreated alloy).

Atom (%)	FeCoNi alloy a	FeCoNi alloy b	FeCoNi alloy c	FeCoNi alloy d
Fe K	30.92	30.94	31.81	31.85
Co K	34.47	34.55	33.95	33.48
Ni K	34.61	34.51	34.23	34.67

Table S3 Elements composition of the prepared FeCoNiO_x electrodes (a', anodized, annealed 100°C; b', anodized, annealed 300°C; c', anodized, annealed 500°C; d', unanodized, annealed 500°C).

Atom (%)	FeCoNiO_x electrode a'	FeCoNiO_x electrode b'	FeCoNiO_x electrode c'	FeCoNiO_x electrode d'
O K	55.34	56.36	62.16	61.88
Fe K	13.24	13.14	24.32	29.21
Co K	12.24	11.96	8.27	8.27
Ni K	19.17	18.55	5.25	0.63

Table S4 Electrochemistry parameters of alloy oxides electrodes.

	Tafel slope (mV/dec)	Overpotential (mV)
Anodized FeCoNi, annealed 100°C	37	170
Anodized FeCoNi, annealed 300°C	83	210
Anodized FeCoNi, annealed 500°C	122	250
Unanodized FeCoNi, annealed 500°C	201	350
Anodized FeNi, annealed 100 °C	33	220
Anodized FeCo, annealed 100 °C	67	250
Anodized CoNi, annealed 100 °C	141	290

C. Supplementary References

1. R R. D. L. Smith, M. S. Prevot, R. D. Fagan, Z. P. Zhang, P. A. Sedach, M. K. J. Siu, S. Trudel and C. P. Berlinguette, *Science*, 2013, **340**, 60-63.
2. L. Kuai, J. Geng, C. Y. Chen, E. J. Kan, Y. D. Liu, Q. Wang and B. Y. Geng, *Angew Chem Int Edit*, 2014, **53**, 7547-7551.
3. (a) D. Gong, C. A. Grimes, O. K. Varghese, W. C. Hu, R. S. Singh, Z. Chen and E. C. Dickey, *J. Mater. Res.*, 2001, **16**, 3331-3334; (b) D. Gong, C. A. Grimes, O. K. Varghese, W. C. Hu, R. S. Singh, Z. Chen and E. C. Dickey, *J. Mater. Res.*, 2001, **16**, 3331-3334.
4. L. A. Marusak, R. Messier and W. B. White, *J. Phys. Chem. Solids*, 1980, **41**, 981-984.
5. S. Trudel, G. Z. Li, X. Zhang and R. H. Hill, *J. Photopolym. Sci. Technol.*, 2006, **19**, 467-475.
6. (a) L. D. Kock and D. De Waal, *Spectrochim. Acta Part A*, 2008, **71**, 1348-1354; (b) I. V. Chernyshova, M. F. Hochella and A. S. Madden, *Phys. Chem. Chem. Phys.*, 2007, **9**, 1736-1750.
7. F. Rubio-Marcos, V. Calvino-Casilda, M. A. Banares and J. F. Fernandez, *Chemcatchem*, 2013, **5**, 1431-1440.
8. H. B. Liao, A. Fisher and Z. C. J. Xu, *Small*, 2015, **11**, 3221-3246.
9. T. Young, *Trans. R. Soc. Lond.*, 1805, **95**, 65-87.
10. (a) L. Barbieri, E. Wagner and P. Hoffmann, *Langmuir*, 2007, **23**, 1723-1734; (b) N. Miljkovic and E. N. Wang, *MRS Bull.*, 2013, **38**, 397-406.
11. J. Bao, X. D. Zhang, B. Fan, J. J. Zhang, M. Zhou, W. L. Yang, X. Hu, H. Wang, B. C. Pan and Y. Xie, *Angew Chem Int Edit*, 2015, **54**, 7399-7404.
12. W. T. Hong, M. Risch, K. A. Stoerzinger, A. Grimaud, J. Suntivich and Y. Shao-Horn, *Energ Environ Sci*, 2015, **8**, 1404-1427.